

Speed Sensorless Direct Torque Control for Three-Level Diode-Clamped Inverter Fed Induction Motor Using Adaptive Flux Observer

Mehmet Ali Usta, H. Ibrahim Okumus, Selcuk Guven and Elif Selin Durak

Dept. of Electrical and Electronics Engineering, Karadeniz Technical University, Trabzon
mausta@ktu.edu.tr, okumus@ktu.edu.tr, selcukguven@ktu.edu.tr, eskaraagacli@ktu.edu.tr

Abstract

In this paper, a speed-sensorless direct torque control (DTC) drive for induction motor (IM) is developed using three-level inverter and a comprehensive study is presented. Firstly, three-level neutral-point clamped (NPC) inverter is handled and the switching vectors used in DTC based on switching table are defined. Second, the adaptive flux observer is utilized to estimate the rotor speed and load torque. Observer model of IM is obtained from the equations of IM in stationary reference frame and adaptive scheme for speed estimation is given in detail. The objective of this study is to present a drive system implemented simply and easily. The proposed drive system is verified by the simulation results.

1. Introduction

Recently, induction machines (IMs) are commonly used in the fields of electric vehicle and industrial application. In these variable speed applications, speed and torque control are required, however the control of IMs is considerably more complicated due to the lack of a linear relationship between the machine current and the resulting torque. Up to now, various control techniques have been developed for IMs. In 1971, Field Oriented Control (FOC) of IMs was introduced by F. Blaschke. A recent development in IM control is Direct Torque Control (DTC) developed and presented by I. Takahashi in 1986 [1]. DTC is different in terms of the operation principle from FOC. In principle, DTC-based drives control the torque and flux applying the optimum voltage vectors selected using switching table to inverter directly. So, a very quick and precise torque response is provided and it is preferable in many applications as opposed to FOC. Moreover, DTC does not require the complex frame transformation, current controllers and pulse-width modulation (PWM) modulator in comparison with FOC-based drives.

The concept of DTC based on switching table (ST-DTC) strategy is widely researched and commercialized because it is very simple and easy to be implemented [2]. However, ST-DTC has some drawbacks. Variable switching frequency and occurring ripples in the torque are the main disadvantages of ST-DTC. The torque ripples can be reduced by using various techniques. A popular method among them is DTC based on space vector modulation (SVM-DTC) that ensures to reduce the torque ripples and also obtain a constant inverter switching frequency. Alternatively, some of them involve the use of high switching frequency or changed inverter topology [3]. If high switching frequency is used, switching losses and stress on the semiconductor devices will significantly increase, but it is possible to solve many of these problems when changed inverter topology is used. Multilevel inverter topologies have gained

popularity in medium and high power applications because their semiconductor devices are exposed to a much lower voltage change rates (dv/dt) and also the output voltage includes less harmonic contents. Furthermore, multilevel inverters enable to produce a greater number of voltage vectors in contrast with conventional inverters. It means that the choices of voltage vectors are increased such that it provides more options to select the most appropriate voltage vectors to generate the exact stator voltage. So, the desired changes in the torque and flux are produced with less ripples than traditional inverter.

There are three different topologies for multilevel inverter, but diode-clamped or neutral-point clamped (NPC) multilevel inverter is widely used for ac-drives. In literature, many papers about DTC [4-8] have been performed using three-level NPC inverter. In these studies, different switching tables for three-level inverter are developed by taking into consideration the hysteresis band levels of torque and flux. On the other hand, there are several studies based on fuzzy controller [4,5] instead of using the hysteresis comparators and switching table for the inverter state selection. Additionally, [6] is focused on SVM-DTC method and also discrete SVM-DTC is studied in [7] for IMs fed three-level inverter.

In recent years, speed sensorless drives are attracted more attention because it makes drive systems more robust, reliable and economic due to not require encoder to obtain speed feedback. For a speed-sensorless DTC drive, various techniques have been developed; especially observers and adaptive systems are commonly used to estimate the flux, torque and speed. Some studies about speed-sensorless DTC drive with three-level inverter are given as follows. Speed adaptive flux observer is studied in [7]. As reported in [8], model reference adaptive system (MRAS) is also studied.

The aim of this paper is to achieve high-performance sensorless ST-DTC for a three-level inverter-fed IM drive. This paper is organized as follows. Firstly, three-level NPC inverter is introduced in Section 2, Secondly, induction motor model, mathematical background of speed estimation and ST-DTC is briefly studied in Section 3. Finally, simulation results and conclusions are given in Section 4 and 5, respectively.

2. Three-Level Neutral-Point Clamped Inverter

The simplified circuit diagram of a three-level NPC inverter is shown in Fig. 1. Each inverter leg is composed of four switches S_{x1} to S_{x4} with four antiparallel diodes D_{x1} to D_{x4} . The dc bus voltage V_{dc} is split into two equal parts by the dc bus capacitors C_{d1} and C_{d2} , providing a neutral-point Z . The clamping diodes D_{zx1} and D_{zx2} are connected to the neutral-point. The operating status of the switches in the three-level NPC inverter can be represented by switching states shown in Table 1.

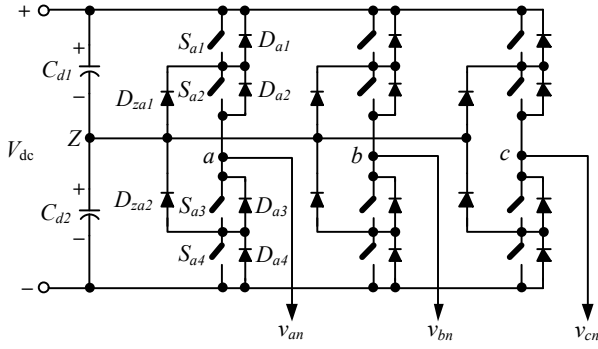


Fig. 1. The circuit diagram of a three-level NPC inverter

Table 1. Switching states of three-level NPC inverter

Switching State	Device Switching Status				Inverter Terminal Voltage
	S_{x1}	S_{x2}	S_{x3}	S_{x4}	
S_x					v_{xz}
p	1	1	0	0	$+V_{dc}/2$
o	0	1	1	0	0
n	0	0	1	1	$-V_{dc}/2$

It can be observed that switches S_{x1} and S_{x3} similarly, S_{x2} and S_{x4} operate in a complementary manner. Switching state p denotes that the upper two switches S_{x1} and S_{x2} are on and the inverter terminal voltage v_{xz} is equal to $+V_{dc}/2$, whereas n indicates that the lower two switches S_{x3} and S_{x4} conduct, leading that v_{xz} is equal to $-V_{dc}/2$. Final switching state o represents that the inner two switches S_{x2} and S_{x3} are on and v_{xz} is clamped to zero through the clamped diodes. Thus, three possible levels of v_{xz} are obtained depending on the choice of switching states.

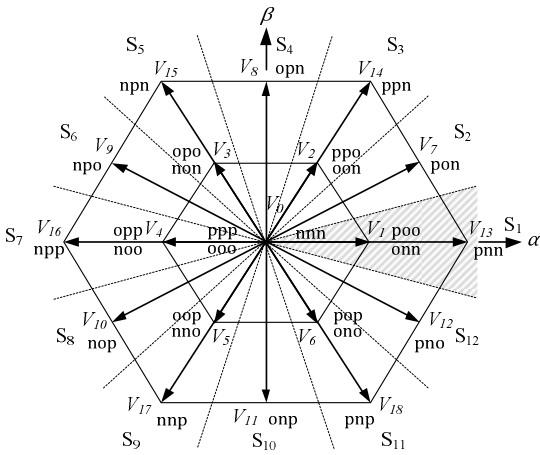


Fig. 2. Space vector diagram for three-level inverter

A three-level inverter generates $3^3 = 27$ switching states as indicated in Fig. 2. In these switching states, although there are 24 active and 3 zero states, some of them apply the same voltage vector. Therefore, 19 different voltage vectors are available as shown in Fig. 2. According to the modulus of each vector, the 19 vectors are classified into four groups: zero vector V_0 , short vectors $V_1 - V_6$, medium vectors $V_7 - V_{12}$ and long vectors $V_{13} - V_{18}$. As shown in Fig. 2, the possible switching

configuration of long and medium vectors is one, but the possible configuration of short vectors are two that is p and n-type. p-type small vector contains p switching state and n-type contains n switching state. Zero vector has three possible state.

The space voltage vector diagram for the three-level inverter is divided into twelve sectors (S_1, S_2, \dots, S_{12}) and the first sector is located in -15° to $+15^\circ$ based on flux angle.

3. Mathematical Background

3.1. Induction Motor Model

The space vectors for the voltage and flux equations of IM in stationary reference frame are given as follows.

$$\bar{v}_s = R_s \bar{i}_s + \frac{d\bar{\psi}_s}{dt} \quad (1)$$

$$0 = R_r \bar{i}_r + \frac{d\bar{\psi}_r}{dt} - jp\omega_m \bar{\psi}_r \quad (2)$$

$$\bar{\psi}_s = L_s \bar{i}_s + L_m \bar{i}_r \quad (3)$$

$$\bar{\psi}_r = L_r \bar{i}_r + L_m \bar{i}_s \quad (4)$$

where \bar{v}_s is the stator voltage, \bar{i}_s, \bar{i}_r are the stator and rotor current, respectively, $\bar{\psi}_s, \bar{\psi}_r$ are the stator and rotor flux, respectively, R_s, R_r, L_s, L_r, L_m are the motor parameters, p is the number of pole-pairs and ω_m is the angular velocity.

The electromagnetic torque T_e is

$$T_e = \frac{3}{2} p \bar{\psi}_s \times \bar{i}_s \quad (5)$$

and also the equation of motion is

$$T_e = T_L + J_L \frac{d\omega_m}{dt} + f_d \omega_m \quad (6)$$

where T_L is the load torque, J_L is the moment of inertia and f_d is the damping coefficient.

3.2. Flux Observer Model of Induction Motor

An IM can be described by the following state equations obtained from Eqns. (1)-(4) in the stationary reference frame.

$$\frac{d}{dt} \begin{bmatrix} \bar{i}_s \\ \bar{\psi}_s \end{bmatrix} = \begin{bmatrix} A_{11} & A_{12} \\ A_{21} & A_{22} \end{bmatrix} \begin{bmatrix} \bar{i}_s \\ \bar{\psi}_s \end{bmatrix} + \begin{bmatrix} B_1 \\ B_2 \end{bmatrix} \bar{v}_s = Ax + Bu \quad (7)$$

$$\bar{i}_s = Cx$$

where $x = [\bar{i}_s \quad \bar{\psi}_s]^T$ and $\bar{i}_s = [i_{s\alpha} \quad i_{s\beta}]^T, \bar{\psi}_s = [\psi_{s\alpha} \quad \psi_{s\beta}]^T$.

$$A_{11} = -\left(\frac{R_s}{\sigma L_s} + \frac{1}{\sigma T_r}\right) I + p\omega_m J = a_{r11} I + a_{i11} J$$

$$A_{12} = \frac{1}{\sigma L_s T_r} I - p\omega_m \frac{1}{\sigma L_s} J = a_{r12} I + a_{i12} J$$

$$A_{21} = -R_s I = a_{r21} I, \quad A_{22} = 0 \quad (8)$$

$$B_1 = \frac{1}{\sigma L_s} I = b_1 I, \quad B_2 = I = b_2 I$$

$$C = [I \quad 0], \quad I = \begin{bmatrix} 1 & 0 \\ 0 & 1 \end{bmatrix}, \quad J = \begin{bmatrix} 0 & -1 \\ 1 & 0 \end{bmatrix}$$

where $\sigma = 1 - L_m^2/L_s L_r$ is the total leakage factor and $T_r = L_r/R_r$ is the rotor time constant. u is the input column vector, $u = \bar{v}_s = [v_{s\alpha} \ v_{s\beta}]^T$, A is the state matrix and is dependent on angular velocity ω_m . B is the input matrix and C is the output matrix.

The state observer, which estimates both the stator current and flux, can be described as follows [9].

$$\frac{d\hat{x}}{dt} = \hat{A}\hat{x} + Bu + G(\hat{i}_s - \bar{i}_s) \quad (9)$$

where $\hat{\cdot}$ denotes estimated values. The estimated state variables are $\hat{x} = [\hat{i}_s \ \hat{\psi}_s]^T$ and $\hat{i}_s = [\hat{i}_{s\alpha} \ \hat{i}_{s\beta}]^T$, $\hat{\psi}_s = [\hat{\psi}_{s\alpha} \ \hat{\psi}_{s\beta}]^T$. G is the observer gain matrix, which is selected so that the system will be stable.

3.3. Adaptive Scheme for Speed Estimation

In a speed-sensorless drive, the speed must be estimated. In this case, the estimated speed is considered as an unknown parameter in the observer model given in Eqn. (9). By adding an adaptive scheme, both states and unknown parameters in the observer can be estimated simultaneously. The speed adaptation has been obtained by using the error dynamics of the system. To obtain the error dynamics, Eqn. (9) is subtracted from Eqn. (7).

$$\frac{de}{dt} = (A + GC)e + \Delta A\hat{x} \quad (10)$$

where $e = x - \hat{x}$ is the estimation error vector and the error state matrix is

$$\Delta A = A - \hat{A} = \begin{bmatrix} p\Delta\omega_m J & -p\Delta\omega_m \frac{1}{\sigma L_s} J \\ 0 & 0 \end{bmatrix} \quad (11)$$

where $\Delta\omega_m = \omega_m - \hat{\omega}_m$. To guarantee the stability of the error dynamics, Lyapunov's stability theorem is utilized. We define the following Lyapunov function V .

$$V = e^T e + \frac{(\omega_m - \hat{\omega}_m)^2}{c} \quad (12)$$

where c is a positive constant. The time derivative of V becomes

$$\frac{dV}{dt} = e^T [(A + GC)^T + (A + GC)]e + (\hat{x}^T \Delta A^T e + e^T \Delta A \hat{x}) - 2 \frac{d\hat{\omega}_m}{dt} \frac{\Delta\omega_m}{c} \quad (13)$$

A sufficient condition for uniform asymptotic stability is that the derivative Lyapunov function is negative definite. If the observer gain matrix G is chosen such that the first term of Eqn. (13) is negative semi-definite, then the adaptive scheme for speed estimation can be found by equating the second and third term in Eqn. (13).

$$2 \frac{d\hat{\omega}_m}{dt} \frac{\Delta\omega_m}{c} = \hat{x}^T \Delta A^T e + e^T \Delta A \hat{x} \quad (14)$$

The error term e_ω is derived from Eqn. (14) as

$$e_\omega = e_{s\alpha} \left(\frac{\hat{\psi}_{s\beta}}{\sigma L_s} - \hat{i}_{s\beta} \right) - e_{s\beta} \left(\frac{\hat{\psi}_{s\alpha}}{\sigma L_s} - \hat{i}_{s\alpha} \right) \quad (15)$$

where $e_{s\alpha} = i_{s\alpha} - \hat{i}_{s\alpha}$ and $e_{s\beta} = i_{s\beta} - \hat{i}_{s\beta}$. Then, the adaptive scheme for the speed estimation is

$$\hat{\omega}_m = K \int e_\omega dt \quad (16)$$

where $K = cp$ is an arbitrary positive gain. The block diagram of the adaptive flux observer is shown in Fig. 3.

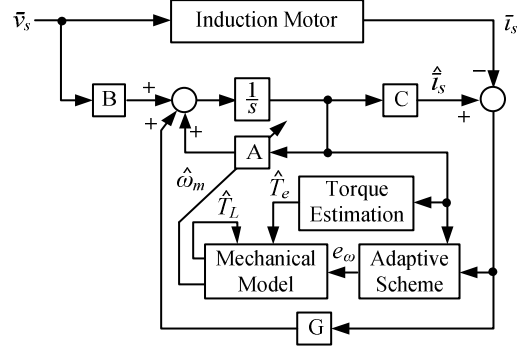


Fig. 3. Block diagram of speed adaptive flux observer

However, in Fig. 3, the following simple mechanical model of the drive is used to improve the response of the speed estimation. This mechanical model is obtained from Eqn. (6) as

$$\begin{aligned} \hat{\omega}_m &= \frac{1}{J_L} (\hat{T}_e - \hat{T}_L) \\ \hat{T}_L &= 0 \end{aligned} \quad (17)$$

where \hat{T}_e is the estimated torque from the adaptive observer and \hat{T}_L is the estimated load torque. In this model, the damping coefficient is neglected, so the load is modeled by a constant load torque [10]. The speed adaptive scheme is used as a correction term for the mechanical model. Thus

$$\begin{aligned} \hat{\omega}_m &= \frac{1}{J_L} \int (\hat{T}_e - \hat{T}_L) dt + K_\omega \int e_\omega dt \\ \hat{T}_L &= -K_T \int e_\omega dt \end{aligned} \quad (18)$$

where K_ω and K_T are arbitrary positive gains.

Now, we design the observer gain matrix G such that all eigenvalues of $A + GC$ have real negative parts. To ensure stability at all speed range, the observer poles are selected in proportional to the machine poles. If the poles of IM are given by λ_{IM} , the observer poles λ_{LO} are selected as

$$\lambda_{LO} = k_p \lambda_{IM} \quad (19)$$

where k_p is the proportionality constant and $k_p > 1$. This makes the observer dynamically faster than IM. When the direct substitution method is used for pole-placement, the gain matrix is obtained as

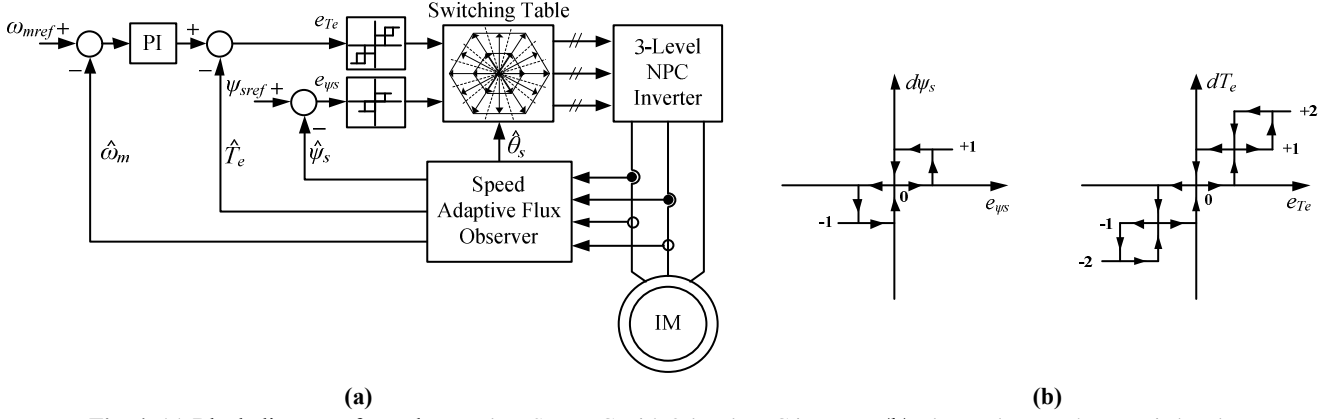


Fig. 4. (a) Block diagram of speed sensorless ST-DTC with 3-level NPC inverter, (b) Flux and torque hysteresis bands

$$G = \begin{bmatrix} g_1 I + g_2 J \\ g_3 I + g_4 J \end{bmatrix} \quad (20)$$

where g_1, g_2, g_3 and g_4 are the observer gains and found as

$$\begin{aligned} g_1 &= (k_p - 1)a_{r11} \\ g_2 &= -(k_p - 1)a_{i11} \\ g_3 &= (k_p^2 - 1)a_{r21} \\ g_4 &= 0 \end{aligned} \quad (21)$$

3.4. DTC for Three-Level Inverter

The principle of DTC is briefly discussed and a torque control for three-level inverter system is studied in this section. The electromagnetic torque can be obtained from Eqn. (5) as

$$T_e = \frac{3}{2} p \frac{L_m}{\sigma L_s L_r} \vec{\psi}_r \times \vec{\psi}_s = \frac{3}{2} p \frac{L_m}{\sigma L_s L_r} \|\vec{\psi}_r\| \|\vec{\psi}_s\| \sin \gamma \quad (22)$$

where γ is the angle between the stator and rotor flux space vectors. When the amplitude of the stator flux is kept constant, the developed torque can be changed by angle γ . From Eqn. (1), if the stator ohmic voltage drops can be neglected, then the

inverter voltage directly controls the stator flux.

$$\Delta \vec{\psi}_s = \vec{v}_s \Delta t \quad (23)$$

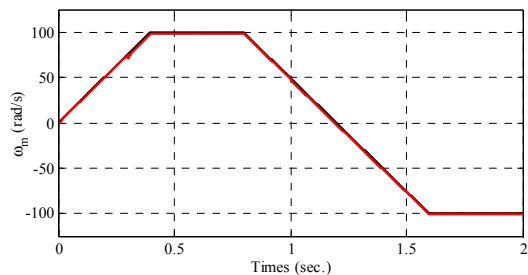
Thus, the required stator flux locus will be obtained by using the appropriate switching vectors. At every sampling period, the switching vectors are selected on the basis of keeping the stator flux error in the 3-level hysteresis band and keeping the torque error in the 5-level hysteresis band. The flux and torque hysteresis bands are depicted in Fig. 4.b. The switching vector selection is tabulated in Table 2 that is taken from [5]. This gives the optimum selection of the switching vectors for all the possible stator flux positions and the desired control inputs which are the reference value of the stator flux modulus and the electromagnetic torque as shown in Fig. 4.a. The estimation of flux, torque and speed used in DTC is carried out by utilizing the adaptive observer illustrated in Fig. 3.

4. Simulation and Results

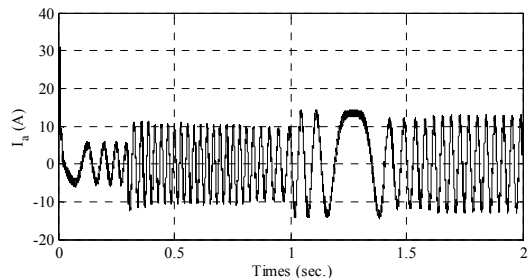
In this section, the validity of the proposed control scheme is examined under different conditions. The sampling frequency is 50 kHz and Runge-Kutta method is used to realize the simulation. The stator flux reference is set to 0.8 Wb. During the simulation, the variable reference speed is applied to the system as shown in Fig. 5.a. A step change of torque command is

Table 2. Switching table of three-level NPC inverter

$d\psi_s$	dT_e	S_1	S_2	S_3	S_4	S_5	S_6	S_7	S_8	S_9	S_{10}	S_{11}	S_{12}
+1	+2	V_7	V_{14}	V_8	V_{15}	V_9	V_{16}	V_{10}	V_{17}	V_{11}	V_{18}	V_{12}	V_{13}
	+1	V_7	V_{2p}	V_8	V_{3p}	V_9	V_{4p}	V_{10}	V_{5p}	V_{11}	V_{6p}	V_{12}	V_{1p}
	0	V_0	V_0	V_0	V_0	V_0	V_0	V_0	V_0	V_0	V_0	V_0	V_0
	-1	V_{12}	V_{1p}	V_7	V_{2p}	V_8	V_{3p}	V_9	V_{4p}	V_{10}	V_{5p}	V_{11}	V_{6p}
	-2	V_{12}	V_{13}	V_7	V_{14}	V_8	V_{15}	V_9	V_{16}	V_{10}	V_{17}	V_{11}	V_{18}
0	+2	V_8	V_{15}	V_9	V_{16}	V_{10}	V_{17}	V_{11}	V_{18}	V_{12}	V_{13}	V_7	V_{14}
	+1	V_8	V_{3p}	V_9	V_{4p}	V_{10}	V_{5p}	V_{11}	V_{6p}	V_{12}	V_{1p}	V_7	V_{2p}
	0	V_0	V_0	V_0	V_0	V_0	V_0	V_0	V_0	V_0	V_0	V_0	V_0
	-1	V_{11}	V_{6p}	V_{12}	V_{1p}	V_7	V_{2p}	V_8	V_{3p}	V_9	V_{4p}	V_{10}	V_{5p}
	-2	V_{11}	V_{18}	V_{12}	V_{13}	V_7	V_{14}	V_8	V_{15}	V_9	V_{16}	V_{10}	V_{17}
-1	+2	V_{15}	V_9	V_{16}	V_{10}	V_{17}	V_{11}	V_{18}	V_{12}	V_{13}	V_7	V_{14}	V_8
	+1	V_{3p}	V_9	V_{4p}	V_{10}	V_{5p}	V_{11}	V_{6p}	V_{12}	V_{1p}	V_7	V_{2p}	V_8
	0	V_0	V_0	V_0	V_0	V_0	V_0	V_0	V_0	V_0	V_0	V_0	V_0
	-1	V_{5p}	V_{11}	V_{6p}	V_{12}	V_{1p}	V_7	V_{2p}	V_8	V_{3p}	V_9	V_{4p}	V_{10}
	-2	V_{17}	V_{11}	V_{18}	V_{12}	V_{13}	V_7	V_{14}	V_8	V_{15}	V_9	V_{16}	V_{10}



(a) Actual and estimated rotor speed



(b) Stator current

Fig. 5. Simulation results of the proposed scheme

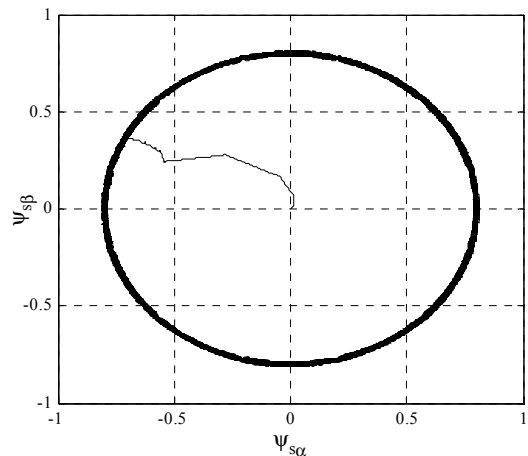
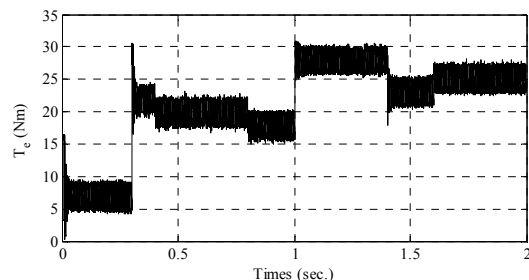


Fig. 6. The stator flux trajectory of machine

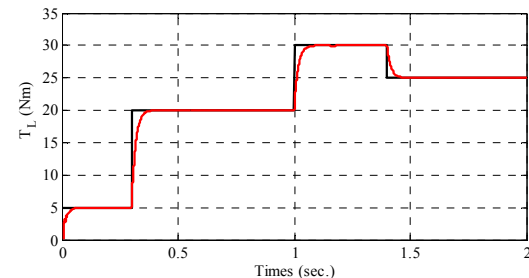
is applied at the beginning of the simulation from 0 to 5 Nm and this command is changed during simulation. Fig. 7.b shows the load torque applied to the system and the estimated load torque. They are given in the same graph for better comparison. The stator current and developed electromagnetic torque of the machine is given in Fig. 5.b and Fig. 7.a, respectively. Fig. 6 shows the trajectory of stator flux.

5. Conclusions

This paper presents speed-sensorless ST-DTC method for a three-level inverter-fed IM drive. Three-level NPC inverter is used to reduce the torque and flux ripples occurred inherently in ST-DTC drive. The speed is estimated using the adaptive flux observer and the load torque is also estimated to improve the speed estimation during speed transients. The proposed scheme is validated by the simulation results. It can be seen that this scheme exhibits fast torque and speed response and very good transient performance is obtained.



(a) Electromagnetic torque



(b) Actual and estimated load torque

Fig. 7. Simulation results of the proposed scheme

6. References

- [1] I. Takahashi, T. Noguchi, "A new quick-response and high-efficiency control strategy of an induction motor", IEEE T Ind Appl, vol. IA-22, no. 5, pp.820-827, Sept./Oct., 1986.
- [2] J.K. Kang, S.K. Sul, "New direct torque control of induction motor for minimum torque ripple and constant switching frequency", IEEE T Ind Appl, vol. 35, no. 5, pp.1076-1082, Sept./Oct., 1999.
- [3] P. Vas, "Sensorless vector and direct torque control", Oxford University Press, New York, USA, 1976.
- [4] S.X. Liu, M.Y. Wang, Y.G. Chen, S. Li, "A novel fuzzy direct torque control system for three-level inverter-fed induction machine", Int J Automot Comput, vol. 7, no. 1, pp. 78-85, Feb., 2010.
- [5] F. Kadri, S. Drid, F. Djeflal, "Direct torque control of induction motor fed by three-level NPC inverter using fuzzy logic", International Conference on Systems and Processing Information, Guelma, Algeria, pp. 1-6, 2011.
- [6] C.H. Krishna, J. Amarnath, S. Kamakshiah, "Simplified SVPWM algorithm for neutral point clamped 3-level inverter fed DTC-IM drive", International Conference on Advances in Power Conversion and Energy Technologies, Mylavaram, pp. 1-6, 2012.
- [7] Y.Zhang, J. Zho, Z. Zhao, W. Xu, D.G. Dorrell, "An improved direct torque control for three-level inverter-fed induction motor sensorless drive", IEEE T Power Electr, vol. 27, no. 3, pp. 1502-1513, Mar., 2012.
- [8] J. Pereda, J. Dixon, M. Rotella, "Direct torque control for sensorless induction motor drives using an improved H-bridge multilevel inverter", 35th Annual Conference of IEEE Industrial Electronics, Porto, pp.1110-1115, 2009.
- [9] H. Kubota, K. Matsue, "DSP-based speed adaptive flux observer of induction motor", IEEE T Ind Appl, vol. 29, no. 2, pp. 344-348, Mar./Apr., 1993.
- [10] J. Maes, J.A. Melkebeek, "Speed-Sensorless direct torque control of induction motors using an adaptive flux observer", IEEE T Ind Appl, vol. 36, no. 3, pp. 778-785, May/June, 2000.